Electronic Supplementary Material (ESI) for Soft Matter

Supplementary information for

Inertia-dependent dynamics of three-dimensional vesicles and red blood cells in shear flow

ZhengYuan Luo [1,2], ShuQi Wang [3], Long He [1,2], Feng Xu [2,4*], BoFeng Bai [1,2 *]

[1] *State Key Laboratory of Multiphase Flow in Power Engineering, Xi'an Jiaotong University, Xi'an 710049, P.R. China*

[2] *Bioinspired Engineering & Biomechanics Center, Xi'an Jiaotong University, Xi'an 710049, P.R. China*

[3] *HST-Center for Biomedical Engineering, Department of Medicine, Brigham and Women's Hospital, Harvard Medical School, Boston 02139, MA, USA*

[4] *The Key Laboratory of Biomedical Information Engineering of Ministry of Education, School of Life Science and Technology, Xi'an Jiaotong University, Xi'an 710049, China*

** Corresponding Author:*

Dr. BoFeng Bai, E-mail: bfbai@mail.xjtu.edu.cn

Dr. Feng Xu, E-mail: fengxu@mail.xjtu.edu.cn

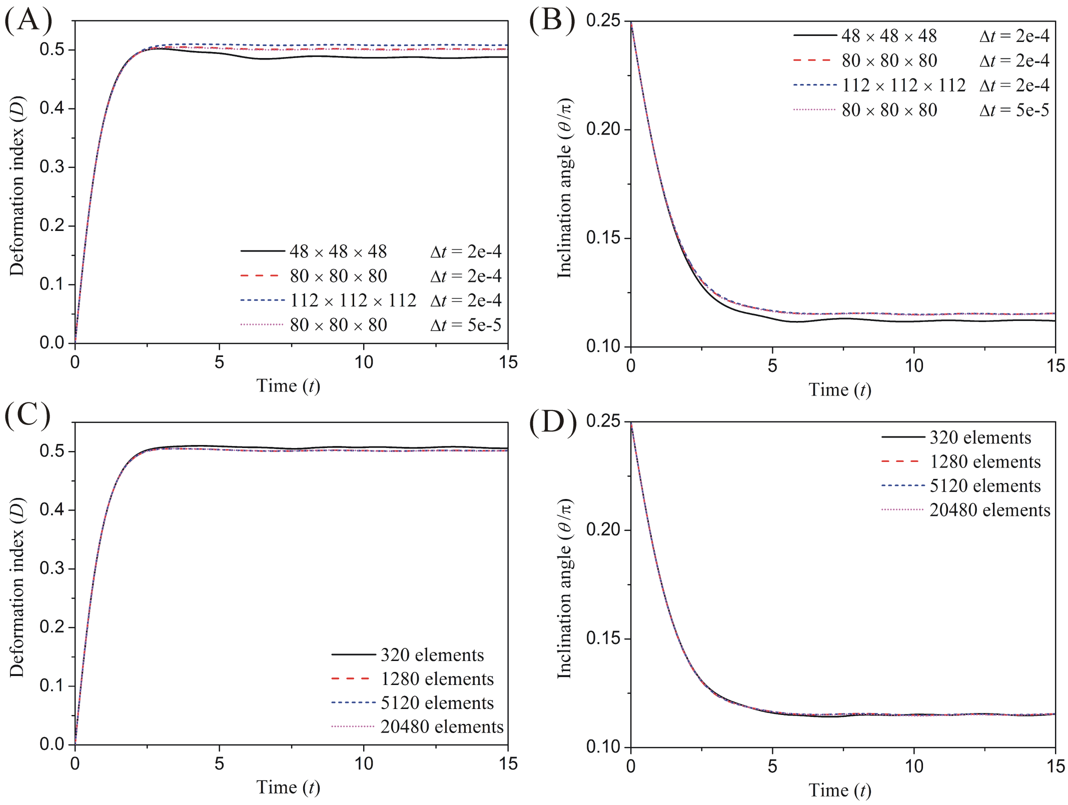

Fig. S1. Numerical performance. To eliminate the effect of the grid resolution, including the Eulerian grid for the velocity field of fluid flows inside and outside vesicles and the Lagrangian grid or the number of triangular elements for the membrane strain and stress field, we performed simulations on behaviors of vesicles with $v = 1$, $\lambda = 1$, Ca = 0.2 and $E_B^* = 0$ at Re = 0.1 under various grid resolutions. (A) and (B) is the temporal evolution of deformation index D and orientation angle θ under various Eulerian grids and time steps. (C) and (D) is the temporal evolution of deformation index D and orientation angle θ under various Lagrangian grids. The Eulerian grid of 10 grids for $1R$, the time step of 2×10^{-4} and the Lagarangian grid of 5120 elements was used for all later simulations in this study.

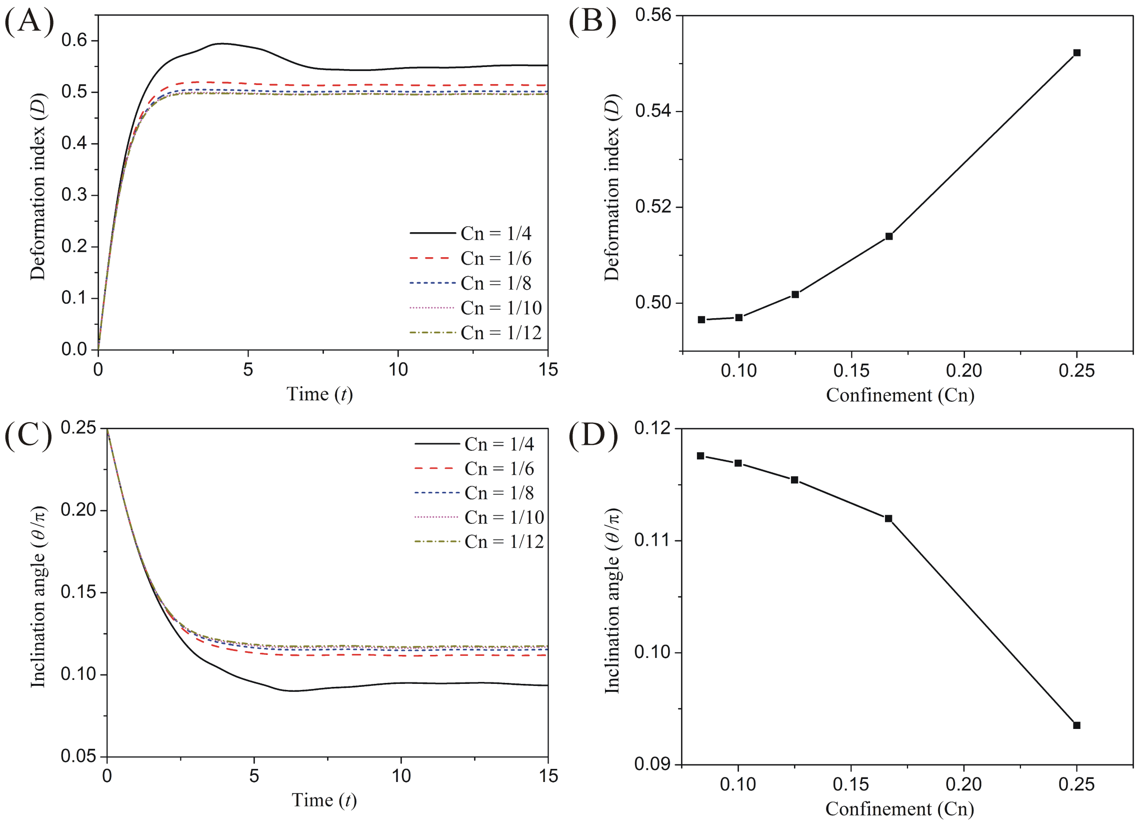

Fig. S2. The effect of vesicle confinement (Cn, the ratio of vesicle size to the distance bwtween the upper and bottom plates). To eliminate the effect of the vesicle confinement, we performed simulations on behaviors of vesicles with $v = 1$, $\lambda = 1$, Ca = 0.2 and $E_B^* = 0$ at Re = 0.1 under various vesicle confinement (Cn = 1/12 − 1/4). (A) and (C) is the temporal evolution of deformation index D and orientation angle θ under various vesicle confinements. (B) and (D) is the equilibrium deformation index D_e and equilibrium inclination angle θ_e as a function of the vesicle confinement Cn. The vesicle confinement has no significant effect on the deformation and orientation of vesicles when Cn < 1/8.

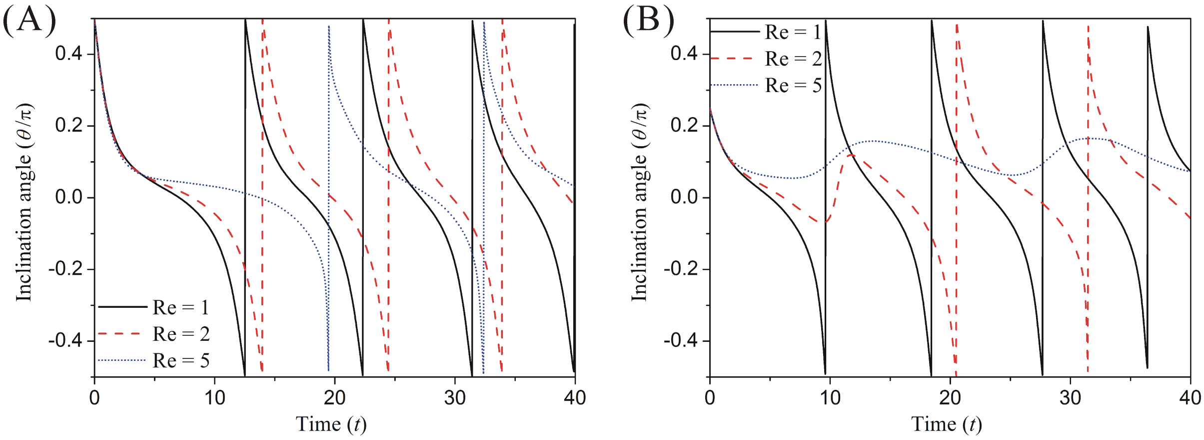

Fig. S3. The inclination angle versus time shows at least three rotations of vesicles or RBCs. (A) RBCs with $\lambda = 10$, Ca = 0.4 and $E_B^* = 0.0025$. (B) Vesicles with $v = 0.87$, $\lambda = 10$, Ca = 0.05 and $E_B^* = 0.05$.

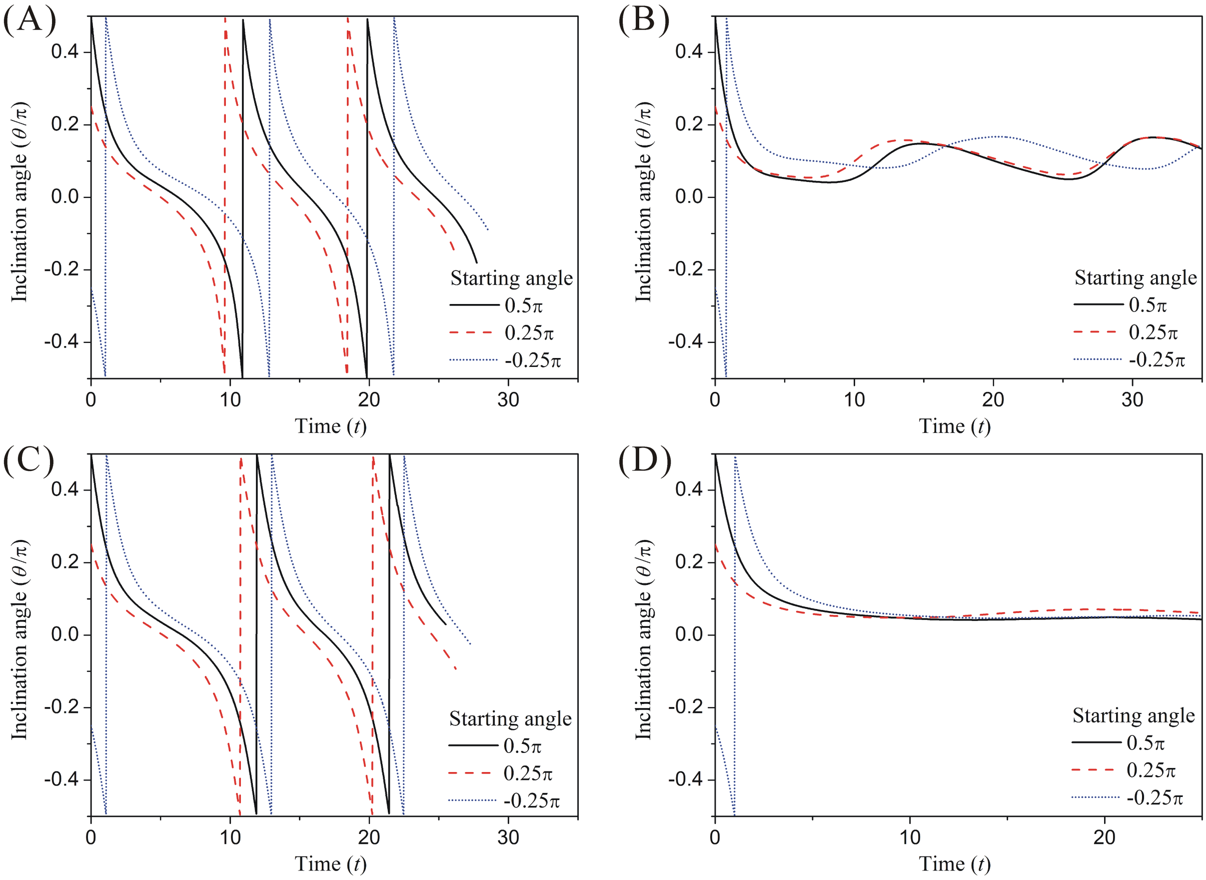

Fig. S4. Dynamics of vesicles or RBCs starting from different initial angles. (A) The tumbling motion of vesicles with v = 0.87, λ = 10, Ca = 0.05 and E_B* = 0.05 at Re = 1. (B) The swinging motion of vesicles with v = 0.87, λ = 10, Ca = 0.05 and E_B* = 0.05 at Re = 5. (C) The tumbling motion of RBCs with λ = 10, Ca = 0.4 and E_B* = 0.0025 at Re = 0.5. (D) The tank-treading motion of RBCs with λ = 4.1, Ca = 4 and E_B* = 0.0025 at Re = 5.

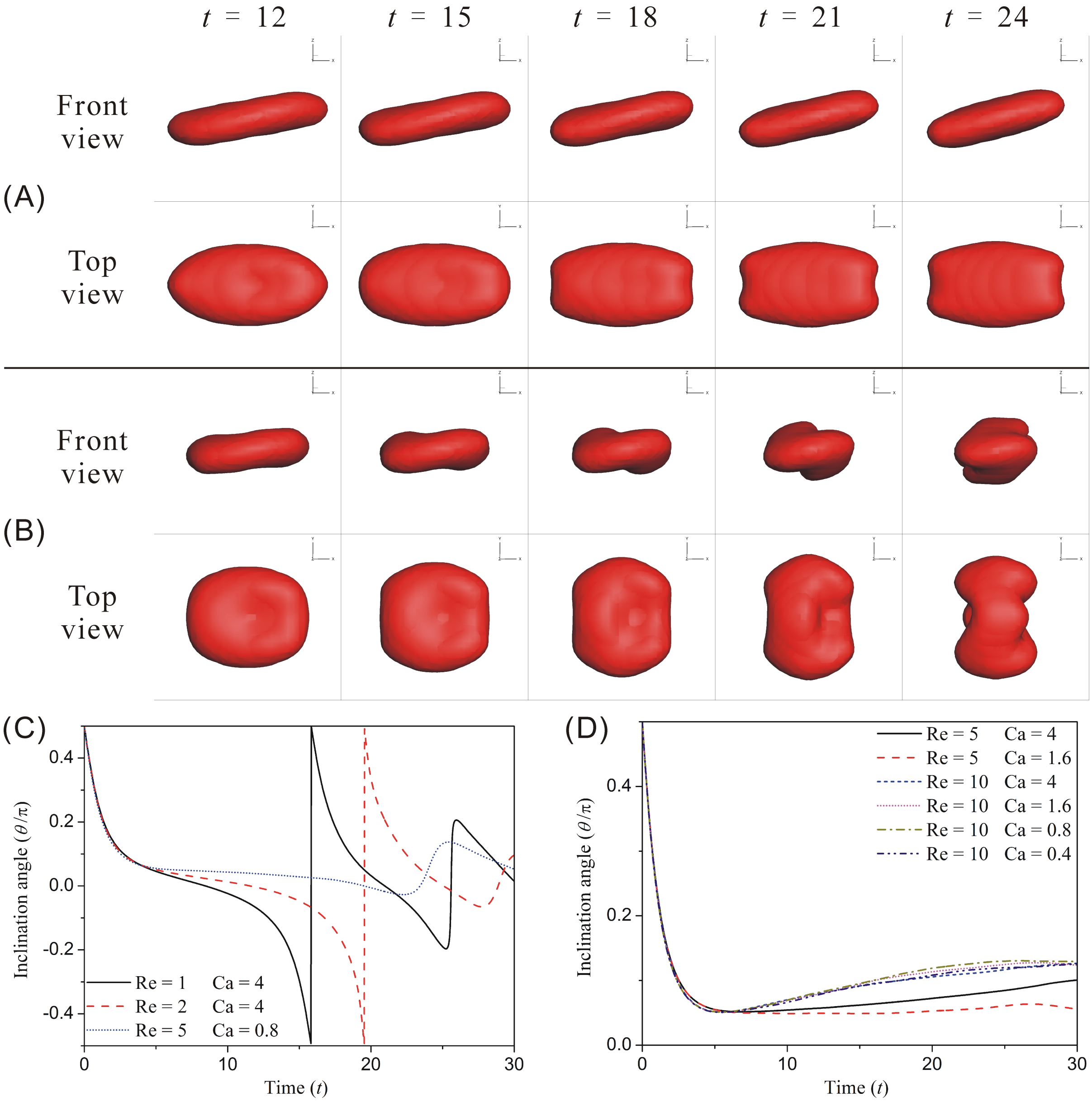

Fig. S5. The differences between the tank-treading and swinging of RBCs at high Reynolds number. The shape evolution of RBCs with λ = 10 and E_B* = 0.0025 at Re = 5 is presented at Ca = (A) 4 and (B) 0.8. The tank-treading and swinging motion is exhibited in (A) and (B), respectively. The inclination angle versus time is presented for RBCs with λ = 10 and E_B* = 0.0025 at (C) swinging (D) tank-treading, respectively.

Video S1: The tumbling motion of oblate-shaped vesicles with $v = 0.87$, $\lambda = 10$, Ca = 0.05 and $E_B^* = 0.05$ at Re = 1.

Video S2: The swinging motion of oblate-shaped vesicles with $v = 0.87$, $\lambda = 10$, Ca = 0.05 and $E_B^* = 0.05$ at Re = 5.